Kramers' turnover theory for diffusion of Na atoms on a Cu(001) surface measured by He scattering

R. Guantes,[a] J. L. Vega, and S. Miret-Artés
Instituto de Matemáticas y Física Fundamental, Consejo Superior de Investigaciones Científicas, Serrano 123, 28006 Madrid, Spain

Eli Pollak
Chemical Physics Department, Weizmann Institute of Science, 76100 Rehovot, Israel

The diffusion of adatoms and molecules on a surface at low coverage can be measured by helium scattering. The experimental observable is the dynamic structure factor. In this article, we show how Kramers' turnover theory can be used to infer physical properties of the diffusing particle from the experiment. Previously, Chudley and Elliot showed, under reasonable assumptions, that the dynamic structure factor is determined by the hopping distribution of the adsorbed particle. Kramers' theory determines the hopping distribution in terms of two parameters only. These are an effective frequency and the energy loss of the particle to the bath as it traverses from one barrier to the next. Kramers' theory, including finite barrier corrections, is tested successfully against numerical Langevin equation simulations, using both separable and nonseparable interaction potentials. Kramers' approach, which really is a steepest descent estimate for the rate, based on the Langevin equation, involves closed analytical expressions and so is relatively easy to implement. Diffusion of Na atoms on a Cu(001) surface has been chosen as an example to illustrate the application of Kramers' theory. © 2003 American Institute of Physics. [DOI: 10.1063/1.1587687]

I. INTRODUCTION

The last years have seen a proliferation of experimental and theoretical studies of atom-surface diffusion.[1–17] The most important questions addressed in such studies, apart from accurate measurements of diffusion coefficients and jump rates, have been the determination of diffusion mechanisms,[2–5] the role played by long jumps in the diffusion process,[6–17] and the detailed knowledge of the adiabatic potential energy surface (PES) which governs the motion of the adsorbed particles.[18–20]

For clean, perfectly periodic surfaces at low coverages, the motion of single adatoms can be probed by different experimental techniques. Field ion microscopy (FIM) and scanning tunneling microscopy (STM) have made possible the study of diffusion on metal surfaces directly at the atomic level,[6–8] providing time-dependent information on the individual displacements carried out by a diffusing adatom. From these measurements, the diffusion coefficients at different temperatures and the time-dependent distribution of adatom locations can be obtained. Their drawback is that they are restricted to relatively low diffusion mobilities ($D \sim 10^{-9}$ cm²/s).

The quasielastic helium atom scattering (QHAS) technique has also been successfully applied to study diffusion of single atoms and molecules on metal surfaces.[18–20] van Hove's formalism for quasielastic neutron scattering[21,22] generalized to surface diffusion[23] can be straightforwardly applied. In contrast to the previous techniques, in which one follows the motion of a single adatom, here, only the ensemble of diffusing particles, as described by a time-dependent distribution function $G(\mathbf{R},t)$, can be probed. At low adatom concentrations, interactions between adsorbates can be ignored, and $G(\mathbf{R},t)$ is defined as the probability of finding a single adatom at the surface position $\mathbf{R}$ at time t, given that it was at the origin at some arbitrary time $t=0$. The observable directly accessible by scattering experiments is the dynamic structure factor, $S(\mathbf{K},\omega)$, which is the Fourier transform in space and time of the function $G(\mathbf{R},t)$. Here $\mathbf{K}$ is the momentum transfer of the helium atoms parallel to the surface and ω the corresponding energy transfer. To obtain information about diffusion coefficients, jump rates, and jump distributions, one generally assumes a diffusion model, valid in a certain wave-vector range under some conditions. For instance, the diffusion coefficients are usually extracted from the behavior of the dynamic structure factor at small $\mathbf{K}$. Low values of the wave-vector transfer imply that the helium beam is probing large distances, thus a continuous diffusion model (no influence of the adiabatic PES) is supposed to be a good description for the diffusion process. On the other hand, as first introduced in this context by Chudley and Elliot,[24] jump distributions and rates are obtained by fitting the whole $\mathbf{K}$ dependence of the quasielastic peak width to an instantaneous jump model (master equation approach).

The remarkable feature of the QHAS technique is that it also allows a direct measurement of low vibrational frequencies of the adatoms. In addition to the quasielastic peak centered at $\omega=0$, a dispersionless mode inelastic peak appears at fixed frequency values of the dynamic structure factor. This peak is related to the frustrated translational mode or

[a]Electronic mail: rgn@imaff.cfmac.csic.es

2780

T-mode, representing vibrations of the adatoms at equilibrium sites. Moreover, the T-mode lifetime, obtained by extrapolation of the T-mode width to surface zero temperature, gives a direct estimation of the friction coefficient[25] between the adatom and the surface. Analysis of the broadening of this peak as a function of the surface temperature and momentum transfer also provides information about the curvature of the PES minima and the anharmonicity. This knowledge has been used in combination with extensive molecular dynamics and Langevin simulations to determine the shape of the adiabatic PES of several systems.[18–20,26]

The good agreement between the simulated data and the experimental values obtained for friction constants, diffusion coefficients, and vibrational frequencies at low adatom concentration allows one to extract some important conclusions for the systems studied. First of all, for barriers $V^{\ddagger} > 3kT$, the diffusion process is activated and the instantaneous jump picture works well. Second, the coupling to the surface is well described in terms of an ohmic friction in the experimentally accessible range of temperatures (between 50 and 300 K). This is an indication that the damping mechanism is mainly due to electron–hole pair creation and/or acoustic phonons.[12,17,18] This is consistent with the fact that the T-mode frequency is lower than the Debye frequency. Third, activation barriers measured from Arrhenius plots of the diffusion coefficient or the quasielastic peak width are always lower than the "static" activation barrier $V^{\ddagger}$ determined from simulation data or from the T-mode frequency.[19,26] This discrepancy has been attributed to several factors: a sizable contribution of long jumps as the surface temperature increases, a failure of the Chudley–Elliot model, or the additional broadening of the quasielastic peak caused by the T-mode contribution, which is not an activated process. Thus static activation barriers obtained from experiment are only reliable if they are measured at low temperatures. Fourth, comparison of the prefactors for the activated jump rates and diffusion coefficients with those given by classical transition state theory (TST) showed large discrepancies.[19] The existence of multiple jumps was again mentioned as a source of error,[27] but only in the context of the Chudley–Elliot model. Last, in order to find agreement between numerical simulations and experiment, a two-dimensional PES with coupling between the two coordinates had to be considered.

A quantum and classical theory of surface diffusion at low coverage, based on Kramers' theory[10] of activated escape over potential barriers was developed by Mel'nikov[28] and Pollak and co-workers.[11,12] This theory provides analytic expressions for the diffusion coefficient, escape rate, and hopping distribution, whenever the underlying dynamics is described in terms of a Langevin equation. The theory provides a steepest descent estimate for the relevant quantities, where the large parameter is the reduced barrier height $V^{\ddagger}/(k_B T)$. The theory has been successfully applied to interpret experimental results of 1D surface diffusion by FIM and STM techniques,[13,14] as well as to analyze the role of multiple hops in activated diffusion.[12,14] For multidimensional problems, it can be also used to study the importance of the coupling between the different degrees of freedom.[14] In this theory, observable quantities such as jump distributions or
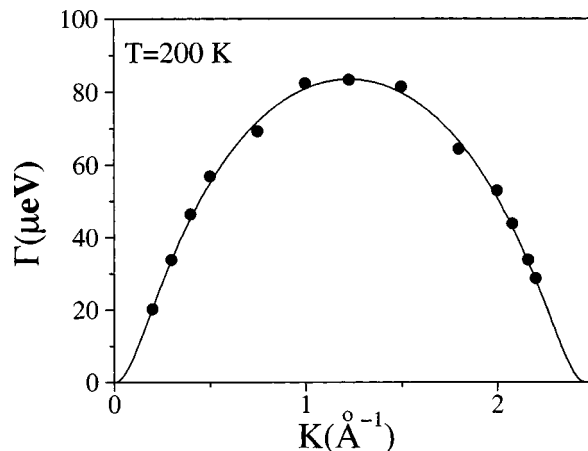

FIG. 1. Half width at half maximum (in μeV) of the quasielastic peak as a function of the wave-vector transfer for the diffusion of Na adatoms on the Cu(001) surface at 200 K. Black circles are the results from the Langevin numerical simulation using a nonseparable interaction potential and the solid line is the least-squares fit of Kramers' theory to the numerical data.

diffusion coefficients are governed by two parameters, namely, the energy loss δ (the average energy loss, in units of kT, of a particle as it traverses the distance between two consecutive barriers) and the escape rate in the spatial diffusion regime Γ_{sd}.

The fact that only two parameters are needed is an important advantage over other existing approaches to fit the experimental data. Random walk models in which the hopping rates to different sites are taken as independent fitting parameters[29] are very often used. In the Kramers based approach, the complete hopping distribution is determined in terms of a single parameter, the energy loss. This does not mean that there Langevin equation simulations are no longer necessary. However, they do demand extensive parametrization of a potential energy surface. In comparison, the Kramers based theory is simple—analytic expressions—and physically transparent. These considerations imply that the theory should be added to the tools used in the analysis of the experimental results and in particular, the full width at half maximum of the deconvoluted quasielastic peak as a function of the wave vector transfer.

That Kramers' approach is viable is demonstrated in Fig. 1, where a fit of Kramers' theory (solid line) to a Langevin simulation (black circles) for the motion of Na atoms on a nonseparable, two-dimensional Cu(001) surface at $T = 200$ K is displayed. In particular, in the numerically exact Langevin simulation, the two physical parameters are known to be $\delta = 1.59$ and $\Gamma_{\mathrm{sd}} = 0.062$ ps^{-1}. The least-squares fit of Kramers' theory to the numerical data gives the values 1.56 and 0.076 ps^{-1}, respectively. This level of accuracy is sufficient to demonstrate that indeed a fit of Kramers' theory to experimental data would lead to a rather accurate determination of the two parameters.

The main purpose of the present article is thus to show that Kramers' theory generalized to surface diffusion provides a good method for analyzing experimental QHAS results and quickly obtaining the relevant information. We will show that even the multidimensional Kramers' theory can be

successfully used provided that the coupling between the different degrees of freedom is not too strong. In the next section we will briefly describe the system and the basic formalism usually employed to obtain the quantities of interest, such as diffusion coefficients or jump distributions, from QHAS experiments. Next, in Sec. III, we discuss Kramers' theory of activated surface diffusion. Then, in Sec. IV, we provide detailed one- and two-dimensional numerical tests of Kramers' theory. We finish with a comparison to available experimental data and some conclusions.

II. THE QUASIELASTIC HELIUM ATOM SCATTERING (QHAS) FORMALISM

A. Potential energy surface

As mentioned earlier, at low adatom coverages, the adsorbate–adsorbate interactions can be disregarded and only the adsorbate–substrate interaction which is governed by a multidimensional PES must be taken into account. For the Na/Cu(001) system, the frequency of vibration along the coordinate perpendicular to the surface is much larger than parallel vibrational frequencies, and the corresponding PES is considered as being averaged over the Na vibrations normal to the surface. Therefore Na atoms move on a two-dimensional, periodic potential. In theoretical simulations of QHAS experiments, two PESs have been proposed.[18,19] The most recent one is nonseparable and was fitted to an expression of the form[19]

$$V(x,y) = V_0(x,y) + V_1(x,y) + V_2(x,y). \tag{1}$$

The first term is a separable cosine potential

$$V_0(x,y) = V_0[2 - \cos(2\pi x/a) - \cos(2\pi y/a)], \tag{2}$$

where a is the lattice constant of the Cu(001) surface ($a = 2.557$ Å), and $V_0 = 41.4$ meV. The second term is added to produce a lowering of the potential barrier in the diagonal direction.

$$V_1(x,y) = -A \sum_{m,n} \exp(-b\{[x/a - (m + \tfrac{1}{2})]^2$$
$$+ [y/a - (n + \tfrac{1}{2})]^2\}) \tag{3}$$

with $A = 2V_0$ and $b = 11.8$. This term was added to account for the experimental observation of a sizable contribution of diffusion paths not going directly over the saddle point.[19] Finally, the third term is a nonseparable part which changes the curvature near the minima and varies the difference between the potential at the minima and the bridge positions,

$$V_2(x,y) = CV_0\pi^2 \sum_{m,n} [(x/a - m)^2 + (y/a - n)^2]$$
$$\times \exp[-(x/a - m)^2 - (y/a - n)^2] \tag{4}$$

with $C = -0.2$.

The four adjustable parameters V_0, A, b, and C were obtained after extensive optimization to give the best fit between the theoretical (Langevin simulation) and experimental values. The x and y directions are taken along the azimuths with indices $[1\bar{1}0]$ and $[110]$, respectively. The energy zero is taken at the minima $(x,y) = (0,0)$ of the po-

tential wells, corresponding to hollow sites. The saddle point energy along the x or y directions, $(x,y) = (\pm a/2,0)$ or $(x,y) = (0, \pm a/2)$, respectively, is at 74.64 meV, and the saddle point energy along the diagonal [100] or [010] azimuths is at 84.49 meV. There appear also small minima on the potential truncated hills corresponding to on-top sites above the copper atoms which are at an energy of 82.74 meV. The maxima at the hill tops are located at 85.51 meV. In the first theoretical simulations of the QHAS experiments for this particular system,[18] a separable potential consisting of only the $V_0(x,y)$ term, Eq. (2), was employed, with a slightly lower saddle point energy (67 meV).

In the present work, we will use both interaction models to calculate diffusion rates and jump distributions in order to reveal the distinctive features emerging from the potential energy coupling. As Kramers' theory of activated diffusion was originally derived for one-dimensional systems, the use of a separable potential will be a good test for the theory. An analytic multidimensional theory along these lines is only available under additional assumptions since, in principle, the energy loss cannot be easily calculated.[14,30,31]

From the point of view of the purely Hamiltonian dynamics, corresponding to motion without friction, the difference between the separable and coupled cases is qualitative. A separable potential gives an integrable Hamiltonian and the classical dynamics consists of only stable orbits. Above the saddle point energy trajectories along the x or y directions propagate in a ballistic way, diffusing freely, and no change of direction or trapping into a well can occur. In contrast, the nonseparable potential gives rise to instabilities and chaos. Trajectories with energies above the diffusion barrier can become trapped for long times in a well, due to the existence of stable rotating orbits not present in the integrable case.[32] Transport properties in analogy to the noisy case can be defined[33] (although the source of randomness is intrinsic here, due only to the classical dynamics without friction and random force) and, depending on the energy, two different transport regimes, normal and enhanced, can arise.[32,34,35]

At low friction and temperature features of the classical dynamics can still survive.[32] Moreover, in the low to intermediate friction regime the analytical solution for the escape rate requires that the energy distribution of particles close to the barrier top depends mainly on the classical action of a trajectory connecting two consecutive saddle points.[28,36,37] Therefore knowledge of the Hamiltonian dynamics may be important in order to establish the validity of Kramers' theory in the turnover region. It is also worth mentioning that different behavior of the diffusion coefficient as a function of friction has been found for separable and nonseparable two-dimensional potentials.[15,17,38]

B. Basic formalism

The observable measured in QHAS experiments is the differential reflection probability (the probability for a projectile helium atom to be scattered into a certain solid angle Ω with an energy exchange $\hbar\omega$) which is proportional to the dynamic structure factor $S(\mathbf{K}, \omega)$ (Ref. 23)

$$\frac{d^2R(\mathbf{K},\omega)}{d\Omega d\omega} = n_d F^2 S(\mathbf{K},\omega). \tag{5}$$

Here, n_d is the diffusing particle concentration on the surface and F is the atomic form factor which depends on the interaction potential between the He atom and the adparticles. As mentioned in the Introduction, the dynamic structure factor has contributions both from the quasielastic peak centered at $\omega=0$, whose broadening is mainly due to the diffusional motion of the adatoms, and from the T-mode vibrations. The contribution of the T-mode to the quasielastic peak will depend on the incident beam energy, the surface temperature, and the parallel wave-vector transfer $\mathbf{K}$, which is controlled by changing the incident angle of the beam with respect to the surface normal. Experimentally it is not possible to separate the vibrational and diffusional motion contributions, although some mechanisms which take advantage of the incident beam conditions have been recently proposed.[39] Nevertheless, a comparison with theoretical predictions is possible by fitting the quasielastic peak to an effective Lorentzian after deconvolution with the instrument response function.[18,19]

In the absence of any numerical simulation, two simple models are customarily used to extract information from the width of the quasielastic peak. The incident He atom wave packet probes the motion of the adatom on a length scale given by $2\pi/\mathbf{K}$. At small wave vector transfer, corresponding to distances much larger than the lattice constant, He atoms are sensitive only to the macroscopic continuous diffusional motion of the adatoms. Then the distribution function $G(\mathbf{R},t)$ obeys the usual diffusion equation, whose solution is well known,[40] and the dynamic structure factor has the Lorentzian form

$$S(\mathbf{K},\omega) = \frac{1}{\pi}\frac{D\mathbf{K}^2}{\omega^2 + D^2\mathbf{K}^4}. \tag{6}$$

Therefore the diffusion coefficient D can be estimated from the full width at half maximum (FWHM) of the quasielastic peak with respect to ω at small $\mathbf{K}$, which should be equal to $\Gamma = 2D\mathbf{K}^2$. Langevin calculations of the diffusion coefficient for the Na/Cu(001) system through the Einstein or Green–Kubo relations

$$D = \lim_{t\to\infty}\frac{1}{4t}\langle|\mathbf{R}(t)-\mathbf{R}(0)|^2\rangle = \lim_{t\to\infty}\int_0^t\langle\mathbf{v}(0)\cdot\mathbf{v}(\tau)\rangle d\tau \tag{7}$$

have shown that Eq. (6) is indeed a good approximation to the dynamic structure factor for $\mathbf{K}<0.2$ Å^{-1}.[19,32]

In order to get the total jump rates and jump distributions from the dynamic structure factor the most widely used model is the master equation approach, which dates back at least to Chudley and Elliot.[24] Here the diffusion process is assumed to be activated, residence times inside a well are much longer than the velocity correlation time $\tau_v \sim 1/\gamma$, with γ the friction coefficient, and jumps between different sites are considered to be instantaneous. The Fokker–Planck dynamics can then be approximated by a discrete master equation which is solved by Fourier transformation.[24,41] In this

case the dynamic structure factor is again a Lorentzian with respect to ω, and the FWHM is related to the total jump rate and jump probabilities as

$$\Gamma(\mathbf{K}) = 2\kappa\sum_{\mathbf{j}} P_{\mathbf{j}}[1-\cos(\mathbf{j}\cdot\mathbf{K})]. \tag{8}$$

κ is the total jump rate out of an adsorption site and $P_{\mathbf{j}}$ the relative probability for a jump with a displacement vector $\mathbf{j}$. Note that Eq. (8) is in fact a cosine Fourier series, so that using the inversion formula for the Fourier coefficients, the total jump rate and jump distributions along specific x or y directions can be obtained from the FWHM as

$$\kappa = \frac{a}{2\pi}\int_0^{\pi/a}\Gamma(K_{x,y})dK_{x,y}, \tag{9}$$

$$P_j = -\frac{a}{k\pi}\int_0^{\pi/a}\Gamma(K_{x,y})\cos(ajK_{x,y})dK_{x,y}, \tag{10}$$

where P_j is now the probability of jumping over j lattice sites in a single jump along the x or y direction and $K_{x,y}$ is the wave-vector transfer in this direction.

Ideally, if one has enough experimental points in the first Brillouin zone of $\mathbf{K}$, this inversion procedure can be accomplished to obtain the rates and jump distributions. In practice one has two sources of error: first, the instantaneous jump picture (for a one-dimensional cosine potential) is a good approximation only for barriers $V^{\ddagger}/kT \geqslant 3$.[42] Second, and more importantly, the FWHM is not really a periodic function of $\mathbf{K}$ whose period is a reciprocal lattice vector,[18,19] as suggested by Eq. (8). This is due to the fact that at large values of wave-vector transfer the contribution of the vibrational T-mode to the quasielastic peak width is appreciable, and diffusional and vibrational motions cannot be separated. In this case, a more reliable way of obtaining information from experiments is by numerically simulating the dynamic structure factor. This can be achieved with molecular dynamics simulations;[26] by a direct numerical solution of the corresponding Fokker–Planck equation (a Klein–Kramers equation in this case) for the distribution function $G(\mathbf{R},t)$;[38,42,43] by application of the Mori projection operator formalism to a microscopic lattice dynamics Hamiltonian;[44] or by simulating stochastic trajectories directly from a Langevin equation.[15,19] Obviously the last three methods should give equivalent results, although a particular choice may be more convenient for practical reasons. For instance, a matrix continued fraction solution[43] of the Klein–Kramers equation is more slowly convergent at low friction values, and difficult in more than one dimension, while the opposite happens with a Langevin simulation: propagation times and size of the ensembles need to be considerably increased at high friction values (and low temperatures), but the added degrees of freedom do not pose a numerical bottleneck.

In order to test the analytical predictions of Kramers' turnover theory we will solve the Langevin equation for a particle in an external field of force with constant (ohmic) friction:

$$\ddot{\mathbf{R}} = -\frac{1}{m}\nabla_{\mathbf{R}}V(\mathbf{R}) - \gamma\dot{\mathbf{R}} + \frac{1}{m}\mathbf{F_r}(t), \tag{11}$$

where V is the adiabatic adsorption potential, Eq. (1), γ is the friction coefficient, and $\mathbf{F_r}$ a Gaussian white noise with zero mean and autocorrelation function

$$\langle \mathbf{F_r}(t)\mathbf{F_r}(t')\rangle = 2m\gamma k_B T \delta(t-t'). \tag{12}$$

The relevant physical observable are obtained by suitable averaging over stochastic paths and time. For instance, the diffusion coefficients can be calculated through any of the equivalent relations (7), and the dynamic structure factor can be obtained from[22]

$$S(\mathbf{K},\omega) = \int dt e^{-i\omega t}\langle e^{-i\mathbf{K}\cdot\mathbf{R}(t)}e^{i\mathbf{K}\cdot\mathbf{R}(0)}\rangle. \tag{13}$$

The numerical method chosen here to integrate the Langevin equation (11) is a third-order velocity Verlet,[45] which converges rapidly even when compared to methods of superior accuracy, such as fourth order Runge-Kutta.[46]

III. KRAMERS' BASED THEORY OF ACTIVATED SURFACE DIFFUSION

A. One-dimensional theory

In Refs. 11, 12, and 28 a semiclassical and classical theory of activated surface diffusion in one dimension was developed, which generalizes Kramers' solution for the problem of escape from a metastable well.[10,28,36,47] The theory is valid for the whole damping range, from the energy diffusion regime to the high friction or spatial diffusion regime, under the following assumptions: the dynamics is described by a Langevin equation; the (reduced) barriers for diffusion are high ($V^{\ddagger}/kT \gg 1$); the potential at the barrier top is approximately parabolic, with frequency $\omega^{\ddagger}$; and energy loss to the bath of trajectories close to the barrier top is given by classical mechanics. We stress (as also shown below) that for a one-dimensional Langevin equation, the Kramers' based theory with finite barrier correction terms can replace the numerical simulation, provided that the reduced barrier height is of the order of ~ 3 and higher.

The starting point for the evaluation of the escape rate, jump distribution, and diffusion coefficient is an equation for the stationary flux of particles exiting each well at either barrier:

$$f_j^+(\epsilon) = \int_{-\infty}^{\infty} d\epsilon' P(\epsilon|\epsilon')[\theta(-\epsilon')f_j^-(\epsilon')$$
$$+ f_{j-1}^+(\epsilon')\theta(\epsilon')], \tag{14}$$

where f_j^+ (f_j^-) are the number of particles per unit energy and per unit time hitting the right(left) barrier of the jth well with positive (negative) velocity, $\theta(x)$ the unit step function, and the kernel $P(\epsilon|\epsilon')$ is the probability that the particle changes its (reduced) energy from ϵ to ϵ' as it traverses from one barrier to the next. The kernel has been shown to have the Gaussian form[28,36]

$$P(\epsilon|\epsilon') = \frac{1}{\sqrt{4\pi\delta}}\exp\left[-\frac{(\epsilon-\epsilon'+\delta)^2}{4\delta}\right], \tag{15}$$

where δ is the (reduced) average energy loss from the particle to the bath. To first order in the damping and the barrier

height the energy loss is simply $\delta = \gamma S/kT$, where S is the classical action of the trajectory which crosses one unit cell at an energy equal to the barrier energy. For a single cosine potential like the one in Eq. (2), with barrier height $V^{\ddagger} = 2V_0$, the energy loss is given by

$$\delta = \frac{8V_0\gamma}{kT\omega_0}, \tag{16}$$

where $\omega_0 = 2\pi\sqrt{V_0/ma^2}$ is the harmonic frequency of oscillation near the well bottom.

To obtain escape rates and jump distributions, the partial rates Γ_j are defined as the number of particles per unit time exiting the zeroth well which are then *trapped* in the jth well. They are given by the difference between incoming and outgoing fluxes:

$$\Gamma_j = \int_0^{\infty} d\epsilon [f_{j-1}^+(\epsilon) + f_{j+1}^-(\epsilon) - f_j^-(\epsilon) - f_j^+(\epsilon)]. \tag{17}$$

Finally, one needs to solve Eqs. (14) and (17) subject to the boundary condition

$$f_j^+(\epsilon) \simeq \delta_{j0}\frac{\omega_0\lambda^{\ddagger}}{2\pi\omega^{\ddagger}}e^{-(\epsilon+V^{\ddagger})} \quad \epsilon \to -\infty \tag{18}$$

which implies that, initially, all the population is in the well $j=0$ and has a thermal distribution of energy close to the bottom of the well. Here $\omega^{\ddagger}$ is the harmonic barrier frequency. Note also that the Kramers–Grote–Hynes prefactor

$$\frac{\lambda^{\ddagger}}{\omega^{\ddagger}} = \sqrt{1 + \frac{\gamma^2}{4\omega^{\ddagger 2}}} - \frac{\gamma}{2\omega^{\ddagger}} \tag{19}$$

appears here as a normalization taking into account recrossings, since we are working in normal mode coordinates for the diffusing particle and the bath.[36]

Equations (14)–(17) with the boundary condition (18) are solved by a discrete Fourier transformation in j followed by a Laplace transformation in energy, for details see Ref. 11. The final result for the partial rates is

$$\Gamma_j = -\frac{\Gamma_{sd}}{\pi}\int_0^{2\pi} dk \sin^2\left(\frac{k}{2}\right)\cos(jk)$$
$$\times \exp\left\{\frac{2}{\pi}\int_0^{\pi/2} dx \ln\left[\frac{1-P^2(x)}{1+P^2(x)-2P(x)\cos(k)}\right]\right\}, \tag{20}$$

where Γ_{sd} is the spatial diffusion escape rate[10]

$$\Gamma_{sd} = \frac{\lambda^{\ddagger}}{\omega^{\ddagger}}\frac{\omega_0}{\pi}e^{-(V^{\ddagger}/kT)} \tag{21}$$

and the function $P(x)$ is given by[48]

$$P(x) = \exp\left[-\frac{\delta}{4\cos^2(x)}\right]. \tag{22}$$

The rate of escape from the zeroth well is

$$\kappa = -\Gamma_0. \tag{23}$$

The relative probability for a jump of length j is given by the probability of being trapped at the jth well:

$$P_j = \frac{\Gamma_j}{\kappa}. \tag{24}$$

For a one-dimensional potential, the diffusion coefficient is related to the escape rate by[41]

$$D = \frac{1}{2} \kappa \langle l^2 \rangle = \frac{1}{2} a^2 \sum_{j=-\infty}^{j=\infty} j^2 \Gamma_j, \tag{25}$$

where $\langle l^2 \rangle$ is the mean squared path length. Introducing Eq. (20) into Eq. (25), the diffusion coefficient can be expressed in the closed form[12,28]

$$D = D_{sd} \Upsilon^{-1} \exp\left\{ \frac{2}{\pi} \int_0^{\pi/2} dx \ln[1 + P(x)] \right\}, \tag{26}$$

where $D_{sd} \equiv 1/2 a^2 \Gamma_{sd}$ is the diffusion coefficient in the spatial diffusion regime, and Υ is the depopulation factor for the metastable well first given by Mel'nikov [see Eqs. (2.55) and (2.56) in Ref. 28]

$$\Upsilon = \exp\left\{ \frac{2}{\pi} \int_0^{\pi/2} dx \ln[1 - P(x)] \right\}. \tag{27}$$

In analogy to the Chudley–Elliot model, an analytical expression for the dynamic structure factor can be obtained by imposing a master equation for the time-dependent distribution $G_l(t)$, which is the probability that the particle is at site l at time t if it was at the zeroth well at $t=0$. Using the partial rates Γ_j this equation takes the form[12]

$$\frac{dG_l(t)}{dt} = \sum_{j=-\infty}^{j=\infty} \Gamma_j G_{l-j}(t) \tag{28}$$

which is solved as usual by Fourier transformation. Defining

$$\hat{\Gamma}(k) = \sum_{j=-\infty}^{j=\infty} e^{ikj} \Gamma_j \tag{29}$$

and using the expression for the partial rates Eq. (20), one readily sees that the dynamic structure factor has the ubiquitous Lorentzian shape with the FWHM given by

$$\Gamma(k) = 2\hat{\Gamma}(k)$$

$$= 4\Gamma_{sd} \sin^2\left(\frac{k}{2}\right)$$

$$\times \exp\left\{ \frac{2}{\pi} \int_0^{\pi/2} dx \ln\left[\frac{1 - P^2(x)}{1 + P^2(x) - 2P(x)\cos(k)} \right] \right\}. \tag{30}$$

It is easy to check by direct substitution of the definitions (23), (24), and (29) that Eqs. (8) and (30) are equivalent. We note, however, that we have identified the probability of a jump of length l in Eq. (8) as $P_l = 2\Gamma_l/\kappa$ since only positive l values are considered and the symmetry condition $\Gamma_l = \Gamma_{-l}$ has been used. Notice also that here k corresponds to the dimensionless wave-vector transfer $aK_{x,y}$ along one specific x or y direction.

Equation (30) is important in the sense that, assuming the validity of Kramers' model and the master equation approach, it allows for a direct comparison with the experimen-

tal data and therefore an estimation of the spatial diffusion rate Γ_{sd} and the energy loss δ. From these parameters and their temperature dependence, one can further infer [via Eqs. (16), (19) and (21)] the barrier height $V^\ddagger$, the friction coefficient γ, and the barrier frequency $\omega^\ddagger$. As will be seen in Sec. III C, finite barrier corrections will mainly affect the prefactor Γ_{sd}.

B. Multidimensional theory

Kramers' turnover theory of activated rate processes has been generalized under certain limitations to many dimensions in Ref. 30. The final equations are formally equivalent to those for the one-dimensional case, but differ in two respects: first, the spatial diffusion rate depends on the force constant matrices at the barrier and the well,[51,52] denoted by $\mathbf{W}^\ddagger$ and $\mathbf{W}_0$, respectively:

$$\Gamma_{sd}^{2D} = \frac{1}{\pi} \left[\frac{\det(\mathbf{W}_0)}{|\det(\mathbf{W}^\ddagger)|} \right]^{1/2} \lambda^\ddagger \exp(-V^\ddagger/kT). \tag{31}$$

The barrier frequency $\lambda^\ddagger$ is the positive solution of the equation

$$\det(\lambda^{\ddagger 2} \mathbf{I} + \lambda^\ddagger \boldsymbol{\gamma} + \mathbf{W}^\ddagger) = 0, \tag{32}$$

where $\mathbf{I}$ is the 2×2 identity matrix and $\boldsymbol{\gamma}$ is the diagonal friction matrix whose elements are the friction coefficients along the unstable and stable directions.

The other difference lies in the energy loss: the parameter δ appearing in the Gaussian kernel (15) depends now on the initial conditions. Strictly speaking, the energy loss and the initial and final energies of the unstable mode, ϵ and ϵ' in Eq. (15), should be averaged over all trajectories initiated at the first barrier with a thermal distribution of energy in the perpendicular stable mode. Therefore application of the multidimensional Kramers' turnover theory calls for a numerical evaluation of the energy loss parameter, which can be computationally as expensive as the calculation of the rate by solving the exact Langevin equation. An analytical estimate for the energy loss is, however, possible in two limits: in the first limit, the two degrees of freedom are strongly coupled through the potential energy function. Motion in the region of the well is then ergodic and then the energy loss turns out[30,49,50] to be proportional to $(V^\ddagger/kT)^2$. In the second weak coupling limit, the separable energy loss (16), proportional to $V^\ddagger/kT$, is a good approximation. If the Langevin dynamics is outside of these two limits, then one has no choice but to resort to full fledged numerical simulations.

C. Finite barrier corrections

When the reduced barrier height $V^\ddagger/kT \lesssim 5$, one must include in the theory finite barrier corrections to the rate expressions.[53,54] The corrections for the spatial diffusion rate are obtained by using the reactive flux method in which the choice of the dividing surface is chosen by minimization of the transition-state flux. Details of the derivation of the resulting expressions can be found elsewhere,[53,54] here we provide only the final formulas for the 2D separable and nonseparable potentials. If the so-called nonlinearity parameter χ is defined as

$$\chi = \frac{(1+\alpha)^2}{\alpha} \tag{33}$$

with $\alpha = \gamma/2\omega^{\ddagger}$, then for a one-dimensional potential, or a 2D separable potential, we have that

$$\Gamma_{\mathrm{fbc}} \simeq \frac{\lambda^{\ddagger}}{\omega^{\ddagger}} \frac{\omega_0}{\pi} e^{-(V^{\ddagger}/kT)} \left[1 - \frac{1}{8\beta} \left(\frac{1}{\chi^2} \frac{V_x^{(4)}(x=a/2)}{[V_x^{(2)}(x=a/2)]^2} \right. \right.$$
$$\left. \left. - \frac{V_x^{(4)}(x=0)}{[V_x^{(2)}(x=0)]^2} \right) \right], \tag{34}$$

where $V_x^{(n)}$ denotes the nth partial derivative of the potential along the reaction coordinate x.

In a similar way, for a 2D nonseparable potential, one finds that the leading finite barrier correction term is

$$\Gamma_{\mathrm{fbc}}^{\mathrm{2D}} \simeq \Gamma_{\mathrm{sd}}^{\mathrm{2D}} \left[1 - \frac{1}{4\beta} \left(\frac{V_x^{(4)}(a/2,0)}{2\chi^2[V_x^{(2)}(a/2,0)]^2} \right. \right.$$
$$+ \frac{V_y^{(4)}(a/2,0)}{2[V_y^{(2)}(a/2,0)]^2} + \frac{V_{x,y}^{(2,2)}(a/2,0)}{3\chi V_x^{(2)}(a/2,0)V_y^{(2)}(a/2,0)}$$
$$- \frac{V_x^{(4)}(0,0)}{2[V_x^{(2)}(0,0)]^2} - \frac{V_y^{(4)}(0,0)}{2[V_y^{(2)}(0,0)]^2}$$
$$\left. \left. - \frac{V_{x,y}^{(2,2)}(0,0)}{3V_x^{(2)}(0,0)V_y^{(2)}(0,0)} \right) \right], \tag{35}$$

where now $V_{x,y}^{(2,2)}$ denotes a crossed second order partial derivative in both directions. Except where stated otherwise, all Kramers' results in this work are understood to be with the inclusion of finite barrier corrections to the spatial diffusion rate.

As shown by Mel'nikov in Ref. 55, the preexponential factor can be also developed in a series in terms of the energy loss parameter in order to take into account finite barrier corrections. However, in the energy diffusion limited regime for $V^{\ddagger}/kT \geq 3$, such corrections are small and so will be neglected.

IV. NUMERICAL RESULTS

A. Separable potential

As a first demonstration of the power of Kramers' based theory, we studied the separable cosine potential case used in the first simulations of the experiment with a barrier of 67 meV.[18] We calculated escape rates, diffusion coefficients, jump distributions, and the dynamic structure factor by solving the Langevin equation for initial ensembles of particles thermalized at the bottom of the potential well. Two approaches were used to numerically determine the rates. One is based on the mean first passage time (MFPT) of the trajectories through a given boundary. For periodic potentials with two equivalent exit paths along each direction, the escape rate in one direction is simply related to the mean first passage time (τ_{MFPT}) by

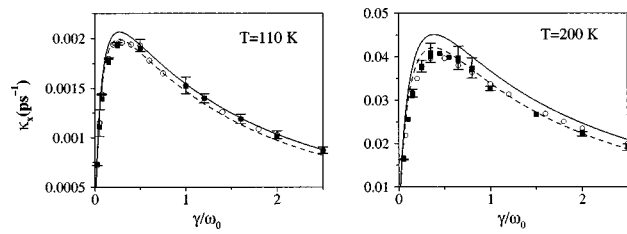$$\kappa = \frac{1}{2\tau_{\mathrm{MFPT}}}. \tag{36}$$

FIG. 2. Escape rates (in ps^{-1}) as a function of the scaled friction for the separable cosine potential, at two different surface temperatures: left panel, $T = 110$ K, and right panel, $T = 200$ K. Kramers' results (solid and dashed lines) are obtained by Eqs. (20)–(23) without and with finite barrier corrections, respectively. Mean first passage time results are plotted with open circles and the closed squares are the corresponding numerical rates obtained by counting jumps.

This relation between the MFPT and the escape rate, as calculated in Kramers' work by the total flux of particles over the initial population of the well, has been demonstrated for the special case of a Gaussian white noise in Appendix B of Ref. 47, and has been recently shown to hold rigorously for arbitrary time-homogeneous stochastic processes.[56] Such a time is almost independent of the precise location of the exit point, as long as it is at a sufficiently remote distance from the barrier to avoid contributions from recrossing trajectories.[27,47]

The second numerical strategy consisted in explicitly determining the jumps between different sites. The rates are then obtained as the total number of jumps of the ensemble, divided by the total propagation time. For numerical purposes, a jump starts when a particle leaves the domain of a unit cell. For the termination of a jump, we employed two different criteria: in one case,[15,27] a jump finishes when its energy is smaller than a prescribed value below the potential barrier in a different potential well; in the other case,[57] the jump terminates when the residence time inside a new well is larger than the characteristic relaxation time (for the low to intermediate friction regime, we typically set it as $2/\gamma$). These criteria are chosen to assure a thermalization of the particle inside a potential well before starting a new jump. Of course, they should give equivalent results within numerical uncertainty.

In Fig. 2 we show the escape rates calculated at two different temperatures: at $T = 110$ K, $V^{\ddagger}/kT \sim 7$ and at $T = 200$ K, $V^{\ddagger}/kT \sim 3.9$, both cases being in the activated regime. The MFPT results are shown as open circles, the black squares with error bars show the rates obtained by counting jumps, the solid line is the theoretical prediction given by Eqs. (23) and (20), and the dashed line corresponds to inclusion of the finite barrier correction. There is a small but noticeable difference between Kramers' theory (solid lines) and the numerical simulation. This difference is mainly due to the fact that the (reduced) barrier height is not sufficiently large and one must take finite barrier corrections into account (dashed lines) for the spatial diffusion limited regime, as described in the previous section. As can be seen, including the finite barrier correction gives good agreement with the simulation results for the whole friction range. From here onwards, all Kramers' based computation will include the finite barrier correction terms.
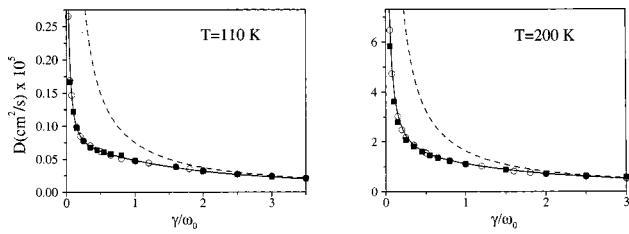
FIG. 3. Diffusion coefficients (in cm²/s) as a function of the scaled friction for the separable cosine potential at two surface temperatures, 110 and 200 K. Solid lines: Kramers' results given by Eq. (26) with finite barrier corrections. Dashed lines: Analytical high friction estimation, Eq. (38). Closed squares: Numerical results using Eq. (25) and the Langevin simulation data for the escape rates and mean squared path lengths. Open circles: Numerical diffusion coefficients from the Einstein relation, Eq. (7).

FIG. 5. FWHM (in μeV) of the dynamic structure factor as a function of the dimensionless wave-vector transfer, $k=a\mathbf{K}$, for the separable cosine potential at $T=110$ and 200 K and $\gamma=0.15\omega_0$. Solid lines: Kramers' results, Eq. (30). Dashed lines: Chudley–Elliott model, Eq. (8), with numerically calculated jump rates and jump distributions. Closed circles: Numerical results obtained by fitting of the simulated dynamic structure factor, Eq. (13), to a Lorentzian shape.

We have also investigated the diffusion coefficients for a wide range of friction values. Analytical predictions for the diffusion coefficient in a periodic potential, apart from Eq. (26), are available only for the spatial diffusion regime[38,57–60] with only nearest neighbor hops. In Fig. 3 the theoretical prediction given by Eq. (26) is plotted as the solid line. Numerical diffusion coefficients are obtained in two ways: through the rates and the mean squared jump lengths, Eq. (25) (closed squares), and using the Einstein relation, Eq. (7) (open circles). For a comparison, we also show with the dashed line the analytical prediction valid in the Smoluchowski limit[38,58]

$$D_x = \frac{D_0 a^2}{\int_0^a dx\, e^{\beta V(x)} \int_0^a dx\, e^{-\beta V(x)}}, \tag{37}$$

where D_0 is the diffusion coefficient in the absence of a potential, $D_0 = kT/m\gamma$. For the separable cosine potential (2), the integrals can be evaluated to yield

$$D_x = \frac{D_0}{I_0^2(\beta V_0)} \tag{38}$$

with $I_0(x)$ the modified Bessel function of order zero.

From molecular dynamics simulations with the separable cosine potential and the experimental T-mode lifetime,[18] the friction coefficient for the Na/Cu(001) system was estimated to be $\gamma \sim 0.15\omega_0$. From Fig. 2 we can see that we are in the turnover region, closer to the low damping regime. At these low damping values, long jumps have been theoretically predicted[13,15,42] and experimentally observed in other systems.[6–8] In Fig. 4 we compare the numerically obtained jump distributions at $\gamma = 0.15\omega_0$ and two different tempera-
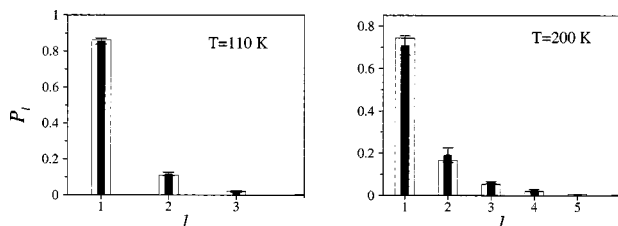
tures (black bars) with the analytical estimation given by Eqs. (20)–(24) (empty bars). Following the previous trends, for the highly activated regime ($T=110$ K) and for $T=200$ K, the agreement in both cases is very good. As expected, the probability of long jumps becomes more important as the temperature is increased.

Finally, we come to the question of how well the FWHM of the quasielastic peak can be reproduced using Kramers' turnover theory and the jump diffusion model. Results are displayed in Fig. 5 at $\gamma = 0.15\omega_0$ and the two previous temperatures. Solid lines are the theoretical prediction and the dashed lines correspond to the Chudley–Elliot model, Eq. (8), with the numerically obtained jump rates and jump distributions. With closed circles we also plot the FWHM obtained from the best fit of the numerically simulated dynamic structure factor, Eq. (13), to a Lorentzian. The very good agreement between the "exact" FWHM and the Chudley–Elliot model at $T=110$ K demonstrates that for high barriers the jump diffusion approximation is excellent. When $V^{\ddagger}/kT < 4$ this approximation deteriorates, as shown in the right panel for $T=200$ K. Moreover, at large wave-vector transfer values we note that purely diffusive contributions cannot be separated so well from vibrational contributions to the quasielastic peak. The analytical FWHM result shows in both cases a small discrepancy around $k=\pi$. In particular, at $T=200$ K, it can be attributed to the worse agreement of single and double jump probabilities with the numerical ones (see Fig. 4) and to the overlapping between the quasielastic and T-mode peaks making the fitting to a pure Lorentzian function more questionable. In this parameter limit, one should complement the Kramers' based theoretical analysis with numerical simulations. Note that for $k=\pi$ the mean free path is $\bar{l}=2a$ and only single and double jumps can be detected.

B. Nonseparable potential

From the previous section we conclude that, for $V^{\ddagger} \geq 4kT$, the Kramers' turnover theory provides a good approximation to the exact Langevin dynamics. All the quantities which can be of experimental relevance are accurately estimated whenever the Langevin equation approach with ohmic damping is a good description of the atom-surface dynamics. Here we will investigate the implementation of

FIG. 4. Probabilities of jumps of length l (in units of the lattice constant a), at $T=110$ and 200 K for the separable potential. Here $\gamma=0.15\omega_0$. Black bars: Numerical results with the corresponding error bars. White: Kramers' results, Eqs. (20) and (24).
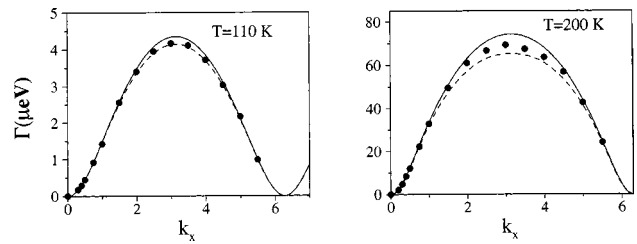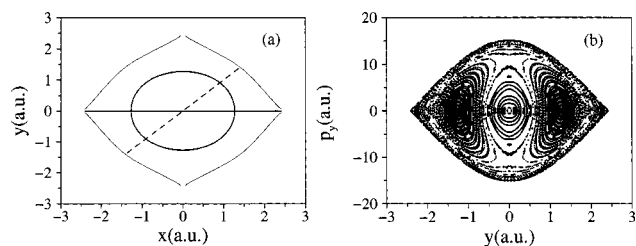
FIG. 6. (a) Main periodic orbits of the Na/Cu(001) system from the non-separable potential at the saddle point energy, 74.64 meV. Solid lines indicate stable orbits and dashed lines unstable ones. The equipotential line at that energy is also shown with thin solid lines to guide the eye. (b) Poincaré surface of section at the middle of the potential well, fixing $x = 0$, for an ensemble of classical trajectories with the barrier energy.

the theory to the 2D problem, that is, when the x and y degrees of freedom are coupled. The semiempirical potential given in Eqs. (1)–(4) will be used for the numerical and analytical comparisons.

As already mentioned, application of Kramers' theory to the multidimensional case is not as straightforward as in one dimension. To apply Kramers' theory, one needs an estimation of the average energy loss δ appearing in the Gaussian probability kernel. The theory is readily applicable only if the coupling between the system modes is either strong or weak. To this end it is necessary to understand the classical dynamics in the absence of friction. Previous detailed studies of the classical dynamics of Na particles moving on this particular PES have shown that for energies above the saddle point chaotic dynamics plays an important role.[32] In fact, statistical properties such as diffusion coefficients can be defined using this deterministic randomness, and they may even display an anomalous behavior depending on the irregularity of the classical dynamics.

The important point here is that by finding the simplest periodic orbits of the system and studying their evolution with energy one can get a very good estimate of the irregularity of the classical dynamics at any energy. The main periodic motions in this system are of three types: two translational orbits parallel to the x and y directions and along diagonal directions, respectively [see Fig. 6(a)], and a rotating orbit of circular type. At the saddle-point energy, the parallel orbits along x or y undergo an abrupt series of bifurcations,[32] since the orbit is no longer localized inside a potential well and free drifting periodic motions of all possible periods become allowed. This also marks a transition to chaotic scattering.[31,33,61] We found, however, that until $E \sim 90$ meV, the parallel and circular motions are stable and influence most of the available phase space of the system. This is illustrated in Fig. 6(b) with a Poincaré surface of section of the system at the saddle-point energy: despite the fact that the diagonal orbit shown in Fig. 6(a) is unstable, most of the phase space is regular with one central chain of stability islands corresponding to the parallel drift motion along x, and two islands to its left and right corresponding to the rotating orbit. Therefore it is reasonable to expect that the separable approximation for the energy loss will work rather well. Indeed, the numerical action across one unit cell for the periodic orbit parallel to the x or y directions is S
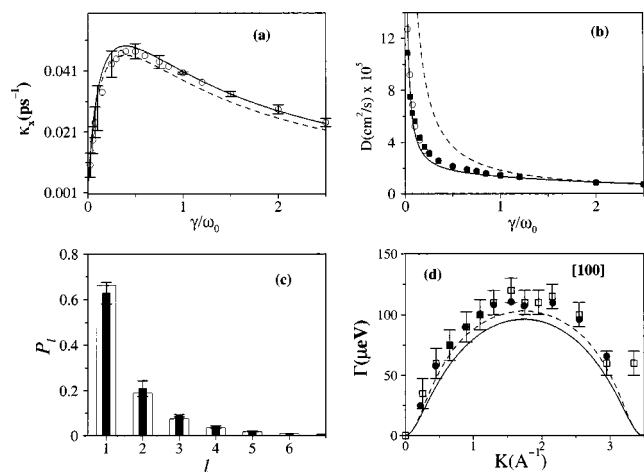

FIG. 7. Results for the nonseparable potential, Eqs. (1)–(4), at $T = 200$ K. (a) Escape rates: solid and dashed lines, Kramers' results, Eq. (20), without and with finite barrier corrections, respectively; open circles, numerical Langevin calculations with error bars. (b) Diffusion coefficients: solid line, Eq. (26); dashed line, quasi-2D approximation Eq. (40); closed squares, numerical results from Eq. (25); open circles, Einstein relation (7). (c) Jump distributions: black bars, Langevin results with error bars; white bars, Eqs. (20) and (24) with $\gamma = 0.1\omega_0$. (d) FWHM of the dynamic structure factor with $\gamma = 0.1\omega_0$: solid line, Kramers' results obtained by Eq. (30); dashed line, Chudley–Elliott model, Eq. (8), with numerical data for the jump rate and jump distributions; closed circles, numerical results from the dynamic structure factor Eq. (13) with error bars; open squares: experimental data taken from Ref. 19 (see text for details).

~ 46.4 a.u., while the action for the separable cosine potential, $S = 4a\sqrt{mV^{\ddagger}/2}/\pi$, with the static barrier height $V^{\ddagger} = 74.64$ meV yields the value $S \sim 46.6$ a.u.

In a similar vein, for weak damping, motion perpendicular to the reaction coordinate is integrable. Therefore we ignore the finite barrier correction terms that come from the perpendicular direction and include from Eq. (35) only the finite barrier corrections along the reaction coordinate (x direction). Including the finite barrier corrections for the perpendicular mode gives qualitatively wrong results, due to the very shallow nature of the potential along the y direction at the top of the barrier. It should be stressed though that this difficulty in estimating from theory the spatial diffusion rate does not mean that the rate does not exist. It only means that due to the relatively high temperature, it is difficult to estimate it from theory without any further assumptions, such as the integrability of motion along this coordinate.

In Fig. 7 we show the results (a) for the directional rate along x, (b) the diffusion coefficient, (c) the jump probabilities, and (d) the FWHM of the dynamic structure factor at $T = 200$ K or $V^{\ddagger}/kT \sim 4.3$. For the escape rates, we included the multidimensional finite barrier correction[53] along the reaction coordinate as described in the previous section and above. The hopping distribution and the FWHM are shown for the value of the friction coefficient $\gamma = 0.1\omega_0$, choosing $\omega_0 = 9$ THz from the T-mode frequency. This is the value given in Ref. 19 for this particular PES after extensive simulations and comparison to experiments. The analytical results are obtained with the average energy loss

$$\delta \sim \frac{4\gamma a}{\pi kT}\sqrt{\frac{mV^{\ddagger}}{2}}. \tag{39}$$

For the diffusion coefficient we also compare with an expression similar to Eq. (37) generalized to two dimensions, called the quasi-2D approximation:[38]

$$D = D_0 a^2 \frac{\int_0^2 dy \left[\int_0^a dx\, e^{\beta V(x,y)} \right]^{-1}}{\int_0^a dy \int_0^a dx\, e^{-\beta V(x,y)}}. \qquad (40)$$

The general agreement is as good as for the separable cosine potential. Note, however, that the coupling, even though it is weak and the classical dynamics for energies below and around the barrier remains very regular, does have an appreciable effect on all observable quantities. Indeed, the directional escape rates are larger than in the separable case and the probability of long jumps also increases, compare to Figs. 2–4. This is due to the fact that the frequency at the barrier along the stable direction is smaller, and the spatial diffusion rate then becomes larger, see Eq. (31). In a more intuitive picture, a lower frequency along the y direction implies that the channel for diffusion along x is wider, and it is easier to cross the barrier.

Another effect induced by the coupling is the lowering of the barrier at the maxima, i.e., for diffusion along the diagonal directions. This implies that at high temperatures other diffusion paths than those along x and y directions may become available. This can be detected from an analysis of the experimental results.[19] In Fig. 7(d) a comparison is shown between the numerical and analytical FWHM and the experimental data taken from Ref. 19. Note that K in Fig. 6(d) is the wave-vector transfer along the diagonal [100] direction (these data are much less affected by experimental error than those along the parallel [110] direction). In order to compare with the Chudley–Elliot model and the results from Kramers' theory we follow a reasoning similar to the experimentalists: if only jumps along the x and y directions were possible, the FWHM $\Gamma(K)$ at the maximum would be twice as large along the diagonal direction than the value along the parallel direction. However, the ratio at the maxima for the azimuths [110]:[100] is here 1:1.4 [estimated in our case from the numerical simulation of the dynamic structure factor (13) along these two different directions]. This indicates that we have a sizable proportion of jumps along diagonal directions. Therefore the results with solid and dashed lines in Fig. 7(d) were calculated with the directional rates and jump distributions along x and then multiplied by 1.4. It can be seen that the agreement of both the Chudley–Elliot model and the analytical prediction are fairly good. Moreover, by varying the static barrier $V^\ddagger$ we found that the best fit of the analytical model to the experimental results was given by $V^\ddagger \sim 72$ meV, only ~ 2.5 meV lower than the estimated value from the Langevin dynamics simulations, and certainly inside the experimental error (around 6 meV) given for the static barrier.[26]

V. CONCLUSIONS

The central conclusion of this work is that Kramers' theory as applied to activated surface diffusion should be used as an added standard tool to fit and interpret experimental results for adatom diffusion at low coverage. Kramers' theory provides a two parameter representation for the FWHM of the quasielastic peak vs the momentum transfer. The two parameters are the spatial diffusion rate and the energy loss. We have shown that (a) the two parameter fit works well with experimental data; and (b) when applied to a Langevin model for which the barrier in units of kT is not too low, the fit agrees well with the theoretical determination of the two parameters from the Hamiltonian governing the dynamics of the system. From an experimental point of view, the main practical working expression is given in Eq. (30) where the FWHM is given in terms of the two parameters.

Kramers' approach involves closed analytical expressions and so is easier to implement than Langevin numerical simulations. The resulting fitting procedure is less cumbersome and time consuming. At the same time, the fit leads to two parameters, with direct relation to relevant physical quantities. With this in mind we suggest that this method is of value when interpreting and predicting the experimental results.

In addition, we have also demonstrated that Kramers' turnover theory gives a very good estimate of rates, diffusion coefficients, and jump distributions for diffusion of atoms adsorbed on metal surfaces when the barriers for diffusion are $V^\ddagger/kT > 4$ and finite barrier corrections are included through Eqs. (34) and (35). These conditions can be achieved at room temperature for systems with barriers $V^\ddagger > 100$ meV. For most of the systems studied by the QHAS technique, with exception of the Xe/Pt(111) which has a free gas behavior, surface temperatures in general should be lower but are all inside the experimental capabilities.[20]

A further restriction in theory is that the potential coupling should be weak, in the sense that the classical dynamics around the barrier energy should be mainly regular. This is not so restrictive as one may think, as there is also vast freedom in the choice of the PES used to fit the experimental results, when undertaking Langevin simulations. For instance, a periodic PES representing the atom–surface interaction can always be expressed as a Fourier series with the proper symmetry requirements. For the Na/Cu(001) we can take as well the pure cosine potential

$$V(x,y) = V_0 - V_1 \left[\cos\left(\frac{2\pi x}{a} \right) + \cos\left(\frac{2\pi y}{a} \right) \right]$$
$$+ V_2 \cos\left(\frac{2\pi x}{a} \right) \cos\left(\frac{2\pi y}{a} \right). \qquad (41)$$

With V_0, V_1, and V_2 chosen such that $V(0,0) = 0$, $V(0, \pm a/2) = V^\ddagger$ (energy barrier at the saddle point), and $V(\pm a/2, \pm a/2) = V_m$ (energy barrier at the maxima) this results in $V_0 = V_m/4 + V^\ddagger/2$, $V_1 = V_m/4$, and $V_2 = V_m/4 - V^\ddagger/2$. Now, from experimental data we have an estimation of the friction coefficient $\gamma = 0.9$ THz.[18] The only parameters remaining to be determined in the theory are the saddle-point energy $V^\ddagger$ and the *difference* $V_m - V^\ddagger$. Note that the frequencies needed for the spatial diffusion rate are

$$\omega_{0,x} = \omega_{0,y} = \omega_x^\ddagger = \pi \sqrt{\frac{2V^\ddagger}{ma^2}}, \qquad (42)$$

$$\omega_y^{\ddagger} = \pi \sqrt{\frac{2(V_m - V^{\ddagger})}{ma^2}}. \tag{43}$$

The static barrier $V^{\ddagger} \sim 75$ meV can be determined from the T-mode position ω_0 [see Eq. (42)] and therefore only one parameter remains to be fitted, namely, the energy of the barrier top V_m which determines the frequency along the stable y direction *and* the potential energy coupling. Using Kramers' theory (without the finite barrier correction) we fit the experimental data shown in Fig. 7(d) by varying V_m. The best fit (with the same quality as in Fig. 1) is found with $V_m \sim 90$ meV, a value slightly higher than the previous PES (85 meV) but still far away from the barrier for a separable potential $V_m \sim 150$ meV. In other words, using Kramers' approach, one will find rather accurate physical parameters, which will result in the same answer found when undertaking the Langevin simulations. The only difference is that the Kramers' result is simple and very fast.

Does Kramers' theory replace the necessity of carrying out numerical simulations of the Langevin equations? Yes, if the diffusion is one dimensional and the reduced barrier height is not less than ~ 3. No, if the diffusion process is multidimensional. In this case, one needs to understand the underlying classical dynamics in the absence of friction, and one must make sure that indeed the relevant measured experimental data are in the range in which the Kramers' based theory is applicable. Of course, the whole approach assumes low coverage, that is, that interactions between adatoms do not affect the diffusion.

In summary, we have shown that Kramers' theory is a viable approach for analyzing experimental results on diffusion using the QHAS technique. This does not mean that there are not any questions left. For high temperatures, such that the reduced barrier height is lower than ~ 3 one should include also finite barrier corrections for the energy loss, application of Mel'nikov's theory[55] for finite barrier corrections to the hopping distribution remains to be carried out. The theoretical computation of the spatial diffusion rate from the potential energy surface is not always trivial, the leading order finite barrier correction may not suffice. Kramers' theory assumes that hopping in the x direction is uncorrelated with hopping in the y direction. This assumption is not always true, as may be seen from the fact that the ratio of the maximal rate measured along the [100] direction is not twice as large as that measured along the [110] direction.[19] All this implies that the theory of activated surface diffusion may still have some surprises in store for the future.

ACKNOWLEDGMENTS

[1] J. V. Barth, Surf. Sci. Rep. **40**, 75 (2000).
[2] R. Ferrando, R. Spadacini, G. E. Tommei, and G. Caratti, Physica A **195**, 506 (1993); Surf. Sci. **311**, 411 (1994).
[3] F. Montalenti and R. Ferrando, Phys. Rev. B **58**, 3617 (1998).
[4] A. S. Prostnev, M. A. Kozhushner, and B. R. Shub, Surf. Sci. **336**, 385 (1995).
[5] H. T. Lorensen, J. K. Norskov, and K. W. Jacobsen, Phys. Rev. B **60**, R5149 (1999).
[6] D. C. Senft and G. Ehrlich, Phys. Rev. Lett. **74**, 294 (1995).
[7] T. R. Linderoth, S. Horch, E. Laegsgaard, I. Stensgaard, and F. Besenbacher, Phys. Rev. Lett. **78**, 4978 (1997).
[8] S.-M. Oh, S. J. Koh, K. Kyuno, and G. Ehrlich, Phys. Rev. Lett. **88**, 236102 (2002).
[9] J. Jacobsen, K. W. Jacobsen, and J. P. Sethna, Phys. Rev. Lett. **79**, 2843 (1997).
[10] H. Kramers, Physica (Utrecht) **7**, 284 (1940).
[11] Y. Georgievskii and E. Pollak, Phys. Rev. E **49**, 5098 (1994).
[12] Y. Georgievskii, M. A. Kozhushner, and E. Pollak, J. Chem. Phys. **102**, 6908 (1995).
[13] Y. Georgievskii and E. Pollak, Surf. Sci. **355**, L366 (1996).
[14] E. Hershkovitz, P. Talkner, E. Pollak, and Y. Georgievskii, Surf. Sci. **421**, 73 (1999).
[15] L. Y. Chen, M. R. Baldan, and S. C. Ying, Phys. Rev. B **54**, 8856 (1996).
[16] M. Azzouz, H. J. Kreuzer, and M. R. A. Shegelski, Phys. Rev. Lett. **80**, 1477 (1998).
[17] O. M. Braun and R. Ferrando, Phys. Rev. E **65**, 061107 (2002).
[18] J. Ellis and J. P. Toennies, Phys. Rev. Lett. **70**, 2118 (1993); L. Y. Chen and S. C. Ying, *ibid.* **71**, 4361 (1993).
[19] A. P. Graham, F. Hofmann, J. P. Toennies, L. Y. Chen, and S. C. Ying, Phys. Rev. Lett. **78**, 3900 (1997); Phys. Rev. B **56**, 10567 (1997).
[20] A. P. Graham and J. P. Toennies, Surf. Sci. **427–428**, 1 (1999).
[21] L. van Hove, Phys. Rev. **95**, 249 (1954).
[22] J. P. Hansen and I. R. McDonald, *Theory of Simple Liquids* (Academic, London, 1986).
[23] J. W. M. Frenken and B. J. Hinch, in *Helium Atom Scattering from Surfaces*, edited by E. Hulpke, Springer Series in Surface Sciences Vol. 27 (Springer-Verlag, New York, 1992), p. 287.
[24] C. T. Chudley and R. J. Elliot, Proc. Phys. Soc. London **77**, 353 (1961).
[25] A. P. Graham, F. Hofmann, and J. P. Toennies, J. Chem. Phys. **104**, 5311 (1996).
[26] J. Ellis and J. P. Toennies, Surf. Sci. **317**, 99 (1994).
[27] J. L. Vega, R. Guantes, and S. Miret-Artés, Phys. Chem. Chem. Phys. **4**, 4985 (2002).
[28] V. I. Mel'nikov, Phys. Rep. **209**, 1 (1991).
[29] J. D. Wrigley, M. E. Twig, and G. Ehrlich, J. Chem. Phys. **93**, 2885 (1990).
[30] E. Pollak and E. Hershkovitz, Chem. Phys. **180**, 191 (1994); E. Hershkovitz and E. Pollak, J. Chem. Phys. **106**, 7678 (1997).
[31] E. Hershkovitz and L. Wiesenfeld, J. Chem. Phys. **113**, 4558 (2000).
[32] R. Guantes, J. L. Vega, and S. Miret-Artés, Phys. Rev. B **64**, 245415 (2001); J. L. Vega, R. Guantes, and S. Miret-Artés, J. Phys.: Condens. Matter **14**, 6193 (2002).
[33] P. Gaspard, *Chaos, Scattering and Statistical Mechanics* (Cambridge University Press, Cambridge, England, 1998).
[34] T. Geisel, A. Zacherl, and G. Radons, Phys. Rev. Lett. **59**, 2503 (1987).
[35] J. Klafter, M. F. Shlesinger, and G. Zumofen, Phys. Today **49**, 33 (1996).
[36] E. Pollak, H. Grabert, and P. Hänggi, J. Chem. Phys. **91**, 4073 (1989).
[37] E. Pollak, in *Dynamics of Molecules and Chemical Reactions*, edited by R. E. Wyatt and J. Z. H. Zhang (Dekker, New York, 1996).
[38] G. Caratti, R. Ferrando, R. Spadacini, and G. E. Tommei, Phys. Rev. E **54**, 4708 (1996); Chem. Phys. **235**, 157 (1998).
[39] J. L. Vega, R. Guantes, and S. Miret-Artés (unpublished).
[40] S. Chandrasekhar, Rev. Mod. Phys. **15**, 1 (1943).
[41] G. Wanshtröm, in *Interactions of Atoms and Molecules with Solid Surfaces*, edited by V. Bortolani, N. H. March, and N. P. Tosi (Plenum, New York, 1990), p. 529.
[42] R. Ferrando, R. Spadacini, and G. E. Tommei, Phys. Rev. A **46**, R699 (1992); Phys. Rev. E **48**, 2437 (1993).
[43] H. Risken, *The Fokker-Planck Equation* (Springer, Berlin, 1989).
[44] L. Y. Chen and S. C. Ying, Phys. Rev. B **49**, 13838 (1994).
[45] M. P. Allen and D. J. Tildesley, *Computer Simulations of Liquids* (Clarendon, Oxford, 1987).
[46] E. Hershkovitz, J. Chem. Phys. **108**, 9253 (1998); See also R. L. Honeycutt, Phys. Rev. A **45**, 600 (1992).

[47] P. Hänggi, P. Talkner, and M. Borkovec, Rev. Mod. Phys. **62**, 251 (1990).

[48] The expressions for the second integral in Eq. (20) and the Fourier transform of the kernel, Eq. (22) here are different from the one given usually (Refs. 11, 28, and 36), $P(\tau) = \exp[-\delta(\tau^2 + 1/4)]$, since we have used the change of variable $\tau = \tan x/2$ which is more convenient for a numerical evaluation of the integral.

[49] B. J. Berne, Chem. Phys. Lett. **107**, 131 (1984).

[50] B. J. Matkowsky, Z. Schuss, and E. Ben-Jacob, SIAM (Soc. Ind. Appl. Math.) J. Appl. Math. **42**, 835 (1982); B. J. Matkowsky, Z. Schuss, and C. Tier, *ibid.* **43**, 673 (1983).

[51] J. S. Langer, Ann. Phys. (N.Y.) **54**, 258 (1969).

[52] R. F. Grote and J. T. Hynes, J. Chem. Phys. **74**, 4465 (1981); **75**, 2191 (1981).

[53] A. M. Berezhkovskii, E. Pollak, and V. Yu. Zitserman, J. Chem. Phys. **97**, 2422 (1992).

[54] P. Talkner and E. Pollak, Phys. Rev. E **47**, R21 (1993); E. Pollak and P. Talkner, *ibid.* **47**, 922 (1993).

[55] V. I. Melnikov, Phys. Rev. E **48**, 3271 (1993).

[56] P. Reimann, G. J. Schmid, and P. Hänggi, Phys. Rev. E **60**, R1 (1999).

[57] G. Constantini and F. Marchesoni, Europhys. Lett. **48**, 491 (1999); M. Borromeo and F. Marchesoni, Surf. Sci. **465**, L771 (2000).

[58] S. Lifson and J. L. Jackson, J. Chem. Phys. **36**, 2410 (1962).

[59] L. Gunther, M. Revzen, and A. Ron, Physica A **94**, 367 (1979).

[60] P. Reimann, C. Van den Broeck, H. Linke, P. Hänggi, J. M. Rubi, and A. Pérez-Madrid, Phys. Rev. Lett. **87**, 010602 (2001).

[61] E. Ott, *Chaos in Dynamical Systems* (Cambridge University Press, Cambridge, England, 1993).